Negative effective surface viscosities in insoluble fatty acid monolayers: Effect of phase transitions on dilational viscoelasticity

Joanna Giermanska-Kahn,[1] Francisco Monroy,[2,*] and Dominique Langevin[2]
[1]*Centre de Recherche Paul Pascal, CNRS, av. A. Schweitzer, Château Brivazac, F33600 Pessac, France*
[2]*Laboratoire de Physique des Solides, Bâtiment 510, Université Paris-Sud, F91405 Orsay, France*
(Received 5 March 1999)

The viscoelastic properties of insoluble monolayers have been investigated by the excited electrocapillary waves method. Effective negative values of dilational viscosities have been obtained in the liquid expanded and liquid condensed phases of insoluble monolayers of myristic, pentadecanoic, and stearic acids. However, the surface viscosity remains positive for the more expanded monolayers of ethyl palmitate ester. Possible origins of such a behavior are discussed in terms of transitional effects between the two-dimensional coexisting phases. [S1063-651X(99)07712-0]

PACS number(s): 68.10.Et, 47.35.+i, 64.70.−p

I. INTRODUCTION

It is largely admitted that dilational surface viscoelasticity plays an important role in the dynamic behavior of interfaces [1,2]. The properties of foams or emulsions, for instance, are determined by the dynamic behavior of the surfactant monolayers adsorbed at air-water or oil-water interfaces, respectively. Despite the technological importance of these systems, there is a great scarcity of experimental information on the viscoelastic properties of surfactant monolayers. Although the fundamental theoretical background and the main experimental techniques were developed in the 1970s [2–4], some central questions remain unanswered. What are the microscopic mechanisms of coalescence of bubbles or drops? What is the role of surface viscosity in surface stability?

Studies of the propagation of externally excited capillary waves [5–8] or quasielastic surface light scattering from thermally excited capillary waves (QESLS) [9] are among the most convenient methods to examine dilational viscoelasticity. Indeed, capillary waves are coupled to surface longitudinal (soundlike) waves, and the propagation of both types of waves depends upon the dilational viscoelastic coefficients (even though the dependence is much weaker for capillary waves). The external excitation of capillary waves can be carried out by electrocapillary [5,6] or mechanical methods [7,8], in the frequency range 100–1000 Hz. This range can be extended by the light scattering method, where thermally excited waves, with frequencies between 1 kHz and 5 MHz, can be studied.

The dilational properties are obtained from the propagation characteristics of the capillary waves (frequency ω and wavelength λ) via the dispersion equation [3,10]

$$D(\omega)=LT+\omega^2[\eta_1(q-m_1)-\eta_2(q-m_2)]^2=0, \quad (1)$$

with

$$L=\tilde{\varepsilon}q^2+i\omega[\eta_1(q+m_1)+\eta_2(q+m_2)], \quad (2)$$

$$T=\gamma q^2+i\omega[\eta_1(q+m_1)+\eta_2(q+m_2)] - \frac{\rho_1+\rho_2}{q}\omega^2+(\rho_1-\rho_2)g \quad (3)$$

where $q=2\pi/\lambda$ is the wave vector, γ is the surface tension, $\tilde{\varepsilon}$ is the dilational complex elasticity modulus, ρ_i and η_i are the density and viscosity of water ($i=1$) and air ($i=2$), respectively, and $m_i=(q^2-i\omega\rho_i/\eta_i)^{1/2}$ is the inverse penetration depth.

Because of the dissipative effects within the monolayer, the dilational modulus $\tilde{\varepsilon}$ is a complex number, with a real part equal to the actual dilational modulus and an imaginary part equal to the loss modulus, proportional to the dilational viscosity κ [10]:

$$\tilde{\varepsilon}(\omega)=\varepsilon(\omega)+i\omega\kappa(\omega). \quad (4)$$

The complex modulus $\tilde{\varepsilon}$ contains isotropic two-dimensional (2D) compression and in-plane shear contributions. When the monolayer is fluidlike, the shear modulus is zero and the dilational modulus ε is related to surface area variations δA and corresponding surface tension gradients $\delta\gamma$:

$$\varepsilon(\omega)=A\left(\frac{\partial\gamma}{\partial A}\right)_T. \quad (5)$$

The hydrodynamic coupling between capillary and longitudinal surface waves is significant when the ratio $\beta=\varepsilon/\gamma \sim 0.16$, value for which the frequencies of the two types of waves are close. Far from the resonance condition, the coupling is less important and the dilational parameters do not appreciably affect the wavelength and damping of capillary waves. As a consequence, the values of ε and κ cannot be obtained with sufficient accuracy from studies of capillary waves. In practice, capillary wave methods are interesting only for monolayers exhibiting intermediate values of the dilational elasticity (1–40 mN/m). Moreover, in the light

*Author to whom correspondence should be addressed. Permanent address: Departamento de Química Física 1, Facultad de Química, Universidad Complutense de Madrid, Av. Complutense, s/n. E28040 Madrid, Spain.
Electronic address: fmonroy@eucmax.sim.ucm.es

scattering technique, the instrumental broadening introduces a supplementary source of error [9].

The above limitations are not found in studies of longitudinal waves, whose propagation characteristics depend directly on ε and κ. However, these waves can only be excited at low frequencies ($\sim$1 Hz), by means of a mechanical barrier [11,12]. It is difficult to enlarge this frequency range since the wave damping increases with frequency, and overdamping is rapidly reached. On the low frequency side, the wavelength increases and reflection from the trough walls is limiting. Moreover, at these low frequencies, it is not easy to remove the noise background from external mechanical vibrations.

Each of the above experimental methods therefore has its limitations; hence the determination of the viscoelastic coefficients is often affected by large uncertainties. There is an additional reason for the scarcity of experimental data: negative values for the dilational viscosity ($\kappa<0$) are often observed [13–15], and till now there has been no explanation for this strange result. Obviously κ, being a dissipative coefficient, should be positive. This clearly indicates the inadequacy of the current hydrodynamic approach which yields *effective* values for the dilational viscosity when the dilational parameters are obtained from the experiments via the dispersion equation. In the case of soluble monolayers, the presence of adsorption barriers theoretically studied by Velarde and co-workers [16,17] has been frequently invoked in order to explain this anomalous behavior [13–15]. However, the required bulk concentration gradient through the z direction is several orders of magnitude larger than the one resulting from the presence of capillary waves: in the theoretical treatment, a large macroscopic concentration gradient is required to supply the energy transferred to longitudinal (or *Marangoni*) waves [16].

In their recent microscopic description for surface viscoelasticity, Buzza *et al*. [18] showed that effective negative values of the dilational viscosity are also possible in a soluble or insoluble monolayer if the interfacial thickness h becomes comparable to the wavelength of the considered mode ($qh\sim1$). For soluble monolayers, such a condition is equivalent to the macroscopic concentration gradient in the adsorption barrier-driven mechanism [17]. The condition $qh\sim1$ could be fulfilled for a thick polymer layer at the air-water interface, where an interfacial thickness of the order of a micron or larger is easily accessible at high enough molecular weight. Obviously, this cannot be the case for insoluble or soluble monolayers made of small surfactant molecules.

Negative surface viscosities have been reported in numerous light scattering studies performed on soluble monolayers [13–15]. We have also recently found negative viscosities in a series of aqueous solutions of cationic *n*-alkyltrimethylammonium bromides [19], and nonionic *n*-alkyldimethylaminoxides [20] surfactants, depending on the chain length, *p*H, and the ionic force of the subphase, by using electrocapillary excited waves. In all cases, negative values for κ were found only in the frequency range where exchanges between the surface and bulk have no time to occur and where the monolayer behaves as insoluble, i.e., at frequencies larger than the characteristic frequency for diffusive transport between the surface and bulk. In this frequency range, the compression produced by the capillary wave could create a stripelike concentration pattern [21]. If, as a consequence, a simultaneous phase transition occurs, energy can possibly be transferred back to the capillary waves and decrease its damping. If the dissipation is smaller than the one created by viscous losses in the bulk liquid, apparent negative viscosities will be found.

Stripe phases have been frequently observed in certain 2D magnetic systems [21], liquid-crystal films [22], and Langmuir monolayers of fatty acids [23], esters [24], and phospholipid plus cholesterol mixtures [25]. The case of Langmuir monolayers was theoretically addressed in Refs. [26] and [27] Spontaneous stripe phase formation was theoretically predicted in these systems by Hu and Granek [28]. In the absence of molecular tilt, a monolayer at the air-water interface is not expected to produce stripes; however, if a collective tilt is present, as in the case of many condensed phases, stripe or hexagonal phases can form, depending on surface pressure and temperature [28]. This transition is easier in surfactant mixtures because composition modulation is possible [28].

Therefore, and in order to corroborate the correlation between the natural ability to form stripe structures and the appearance of a negative dilational viscosity, we have begun a study of the dynamic rheological behavior of monolayers made with series of insoluble compounds by using the electrocapillary method. We have chosen three homologous fatty acids: tetradecanoic (or myristic acid), pentadecanoic and hexadecanoic (or palmitic acid), and an ester:palmitic ethyl ester, which will be called hereafter C_{14}, C_{15}, C_{16}, and C_{16}Et, respectively. We have chosen these particular compounds because many data for their monolayers already exist in the literature. The phase diagrams of fatty acid monolayers have been studied for almost 60 years, and recently the use of easily washable teflon troughs and commercially available water purification units has improved the data reproducibility between laboratories. Due to the development of fluorescence microscopy (FM) and brewster angle microscopy (BAM), it is also possible to visualize phase coexistence and monolayers morphology. These techniques in conjunction with x-ray diffraction from synchrotron sources have allowed the understanding of the complicated polymorphism of condensed phases [29–32].

The main aim of this work is therefore twofold: first to investigate if negative dilational viscosity also exists in the studied Langmuir monolayers, and then to correlate the viscoelastic parameters with the 2D phase behavior. This paper is organized as follows: Section II summarizes the experimental details. The equilibrium and viscoelastic experimental results are given in Sec. III and are discussed in Sec. IV. Finally, Sec. V summarizes the main conclusions.

II. EXPERIMENT

High purity C_{14} and C_{15} (>99%) were purchased from Fluka and recrystallized four times before use from spectroscopic grade heptane. For both acids we did not notice any significant difference in the viscoelastic parameters between purified and nonpurified material. Therefore, C_{16} (Fluka) and C_{16}Et (Sigma), both with the same nominal purity (>99%), were used without further purification. Langmuir monolayers

were formed on the aqueous subphase by depositing small drops of dilute solutions with a microsyringe (Hamilton). Spectroscopic grade chloroform (Prolabo) was used as spreading solvent and solution concentration fixed around 1 mM. In order to check for the absence of surface active impurities, blank experiments with the pure solvent were performed: after solvent evaporation, surface tension equal to that of the pure subphase and zero viscoelastic parameters are obtained. A given surface concentration Γ was obtained by successive additions to a fixed surface area, $\Gamma = 1/A$, where A is the area per molecule. A few independent series of additions allow the determination of the surface pressure Π variation with surface concentration, called hereafter the ''isotherm;'' $\Pi = \gamma_w - \gamma$, where γ_w is the surface tension of the pure substrate. The fatty acid monolayers were spread upon a 0.01-M aqueous solution of HCl (Carlo Erba) in order to prevent for fatty acid dissociation. Double distilled and deionized water from a milli-Q system was used. The experiments have been carried out in a thermostated room at $T = 22.0 \pm 1.0\,^{\circ}\mathrm{C}$. In order to prevent surface contamination, the teflon Langmuir trough was enclosed in a Plexiglas box. After deposition of the monolayer material, we waited for about 20 min before starting the measurements, in order to ensure full solvent evaporation. The equilibrium surface pressure is measured *in situ* by the Wilhelmy method. The open-frame geometry instead of a plate was chosen in order to avoid wetting problems.

Since $C_{16}Et$ is strongly hygroscopic, the commercial product already contains some quantity of water, very difficult to eliminate by vacuum drying. In order to know the exact surface concentration, the Π-Γ isotherms were slightly shifted in order to obtain a saturation area of 20 $\mathrm{Å}^2$, as found by Harkins and Boyd [33].

The surface rheological experiments were performed by the electrocapillary method. Details of the experimental setup have been extensively described elsewhere [6]. In short, capillary waves are excited by applying an ac potential of frequency $\omega/2$ and amplitude $V_{pp} \sim 500\,\mathrm{V}$ to a metal blade located close to the surface. This forces the surface to oscillate at a frequency ω twice that of the applied potential. A He-Ne laser beam is reflected from the surface and its deflection is followed by a position sensitive photodiode. The whole optical assembly is mounted on a translation stage which allows one to scan the surface deformation along the wave spatial propagation direction. The signal is then filtered with a lock-in amplifier. Finally, the wavelength λ and damping constant α of the capillary waves are deduced from a fit of the signal to a damped sinusoid. In order to obtain the viscoelastic parameters ε and $\omega\kappa$, the dispersion equation [Eqs. (1)–(4)] is solved for $q = -i\,\alpha + 2\pi/\lambda$, and for γ equal to the value simultaneously measured by the Wilhelmy method. The frequency range of this setup is $\nu = \omega/2\pi = 200 - 1000\,\mathrm{Hz}$ for studies at the air-water interface. In the present study, the viscoelastic parameters depend only slightly on frequency, so the frequency has been fixed at 800 Hz for all the measurements.

III. EXPERIMENTAL RESULTS

A. Isotherms

Figure 1 shows a typical isotherm for long chain fatty acids and their *a*-alkyl esters. The succession of phases encountered upon compression of the monolayer at constant

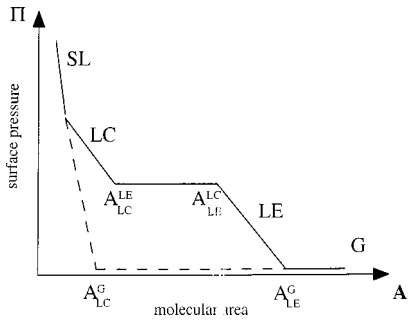

FIG. 1. Typical isotherm for fatty acids and their esters. *G* (gaseous), LE (liquid expanded), LC (liquid condensed) and SL (superliquid) phases are accessible as a function of the monolayer density $\Gamma = 1/A$ and temperature T.

temperature is as follows: gaseous (G), liquid expanded (LE), liquid condensed (LC), superliquid (SL). The two latter are mesophases, intermediate between 2D liquid and solid states. The LC phase is characterized by long-range tilt orientational order and short-range translational order [29]. In some compounds additional transitions between different LC phases have been observed by X-ray diffraction experiments [30,32]. In the SL phase, the tilt vanishes and the molecules are organized in a hexagonal lattice. The absence of molecular tilt in this SL phase favors the internal rotation of the molecule around the chain axis; as a result, the surface viscosity is small in the SL phase [34]. Further compression of the monolayer leads to its collapse, i.e., creation of three-dimensional patches, accompanied by stabilization of the surface pressure.

In Figs. 2(a) and 2(b) the experimental surface pressures measured by the Wilhelmy method during the capillary waves experiments are shown. Since the accuracy of the temperature control is only 1°, the experimental points are scattered. In addition, the scattering increases when the acid chain length decreases, suggesting a possible role of the slow solubilization into the subphase [35]. The lines in Fig. 2 correspond to the experimental data smoothed by filtering through the Savitzky-Golay algorithm. We have also performed continuous compression measurements with the fatty acid samples used in this study [Fig. 2(c)]. With this method, the data scattering is suppressed, and good agreement with the independent measurements of Fig. 2(a) is observed. In the following, we have used the isotherm data of Figs. 2(a) and 2(b) to calculate surface elasticities, since they correspond to the conditions in which the viscoelasticity measurements were made (these measurements last for about 45 min:20 min for spreading and equilibration, 5 min for surface tension measurement, and 20 min for the capillary wave scan).

All isotherms are consistent with literature data: the boundaries between the different phases are given for each compound together with literature data in Table I. The high density limit of the LE phase region is difficult to determine from the isotherms; we have used a criterion based on the observation that in the region of LE-LC coexistence, the dilational elasticity data are strongly scattered. This is due to the heterogeneity of the monolayer, which results in fluctuations of the viscoelastic parameters between the values corresponding to either LC or LE phases. The boundary be-

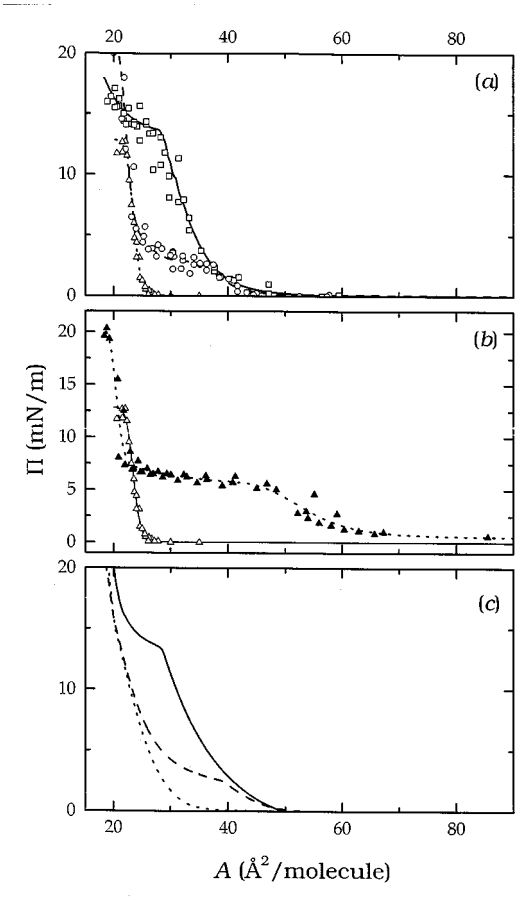

FIG. 2. Experimental Π-*A* isotherms at 22±1 °C for the studied fatty surfactants. (a) Fatty acids: (□) myristic or C_{14}; (○) Pentadecanoic or C_{15}; and (△) palmitic or C_{16}. (b) Comparison between the isotherms of (△) palmitic acid C_{16}, and (▲) its ethyl ester C_{16}Et. (c) Fatty acids, continuous compression method: (——) myristic C_{14}, (— — —) pentadecanoic C_{15} and (· · · ·) palmitic C_{16}. The data in (a) and (b) are independently measured with a Wilhelmy plate.

tween scattered and nonscattered data allows a better determination of the LC phase limit.

The locations of the phase boundaries and the Π values at the LE-LC coexistence plateau are in excellent agreement with literature data [30], and they are fully compatible with the results from FM [22]. The width of the LE-LC coexistence plateau that we find from the isotherm at 22 °C for C_{16}Et is slightly larger than the one found by Harkins and Boyd [33] at 25 °C, as expected, since Π increases with *T*. In the case of C_{16}, the isotherm at 22 °C is already below the triple point, and the LE phase is not present: upon compression, the monolayer goes directly from the gas state to the liquid condensed state when the area is about 26 Å^2 (see Fig. 2). Equivalent conclusions were obtained in the earlier work of Fisher and Sackmann [36].

TABLE I. Coexistence boundaries for the studied Langmuir monolayers. *G* gas; LE, liquid expanded; LC, liquid compressed.

Surfactant	A_{LE}^{G}(Å^2)	A_{LC}^{G}(Å^2)	A_{LE}^{LC}(Å^2)	A_{LC}^{LE}(Å^2)
C_{14}	47[a]		28[a]	22[a]
	52[b]		30[b]	18[b]
C_{15}	45[a]		35[a]	24[a]
	42[c]		37[c]	23[c]
C_{16}		26[a]		
		25[d]		
C_{16}Et	80[a]		42[a]	23[a]
	84[e]		38[e]	24[e]

[a]This work $T=22$ °C.
[b]Reference [46]. $T=22$ °C; data from the phase diagram.
[c]Reference [47]. $T=20$ °C.
[d]Reference [36]. $T=24$ °C; data from the isotherm.
[e]Reference [33]. $T=25$ °C; data from the isotherm.

TABLE II. Equilibrium spreading pressures Π_S of the studied insoluble fatty surfactants at the air-water interface (data at 22 °C from Ref. [37]).

Surfactant	Π_S(mN/m)
C_{14}	17
C_{15}	20
C_{16}	11
C_{16}Et	15

The agreement between the different isotherms is not as good in the condensed states of the monolayer. This is due to the steep slope of the isotherm in this area range, very sensitive to the method by which the density of the monolayer has been changed. With the method of continuous compression, out-of-equilibrium ($\Pi > \Pi_{eq}$) and steeper isotherms can be obtained if the compression velocity of the barriers is too high. If the compression is then stopped, a downfall to the equilibrium pressure is observed as if collapse had occurred. These observations show the strong kinetic effects involved in the formation of 2D condensed states. Metastable states are very frequent, with surface pressures greater than the equilibrium spreading pressure Π_s, defined as the equilibrium pressure between three-dimensional crystals and the monolayer. Table II collects the literature data for Π_s [37] and their comparison with collapse pressures measured in this work by the method of successive additions. With the exception of C_{16}Et, for which the observed collapse pressure is 5 mN/m greater than Π_s, our collapse pressures are equal to Π_s, as expected. It seems that the method of successive additions that we use facilitates the nucleation of the condensed phases, and accelerates equilibration.

The transition to the SL phase of fatty acids observed in Ref. [30] upon compression takes place almost always above the Π_s value. This may indicate that the monolayers are out of equilibrium. In any case, our isotherms are too scattered to distinguish the small kink of the LC-SL transition observed in Ref. [30]. Because of the kinetic dependence of the surface pressure of condensed states, we will instead refer to the molecular area in the description of monolayer states.

There is a particularity concerning C_{14} and its weak but non-negligible solubility in water. A series of additions lasts for a few hours, and during this time there is a certain leakage of the surfactant to the bulk, that leads to small errors in the molecular area. It can be noted in Fig. 2(a) that the denser monolayers were obtained at $A \sim 19$ Å^2, which is probably too low.

Figure 2(a) shows clearly the thermodynamic equivalence between temperature and *n*, the number of carbon atoms of

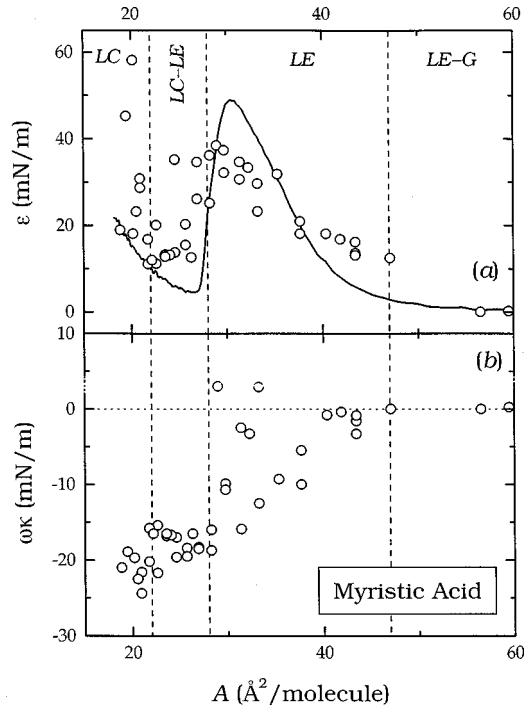

FIG. 3. Experimental viscoelasticity data for the monolayers of myristic acid C_{14} at the air-water interface and at $22\pm1\,^{\circ}C$ as a function of area per monomer. (a) Dilational elasticity modulus $\varepsilon(\omega)$ at $\nu=800$ Hz and comparison with the static value ε_0 (continuous line). (b) Dilational loss modulus $\omega\,\kappa(\omega)$ at the same frequency. The vertical dotted lines delimit the different 2D phases.

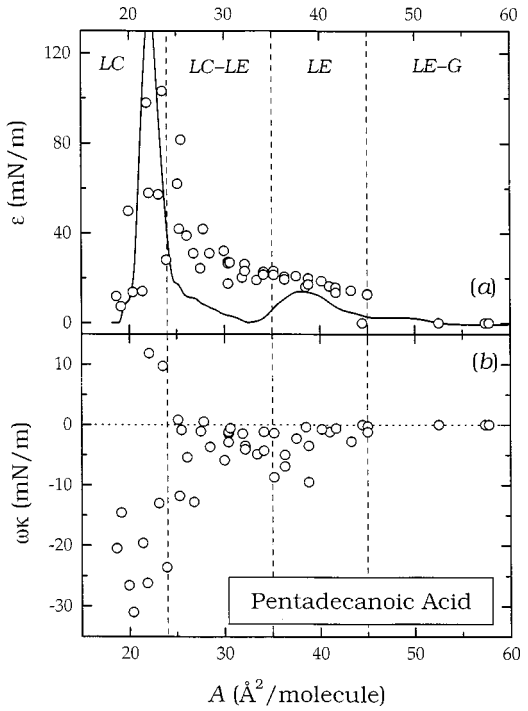

FIG. 4. Experimental viscoelasticity data for the monolayers of pentadecanoic acid C_{15} at the air-water interface and at $22\pm1\,^{\circ}C$ as a function of area per monomer. (a) Dilational elasticity modulus $\varepsilon(\omega)$ at $\nu=800$ Hz and comparison with the static value ε_0 (continuous line). (b) Dilational loss modulus $\omega\,\kappa(\omega)$ at the same frequency. The vertical dotted lines delimit the different 2D phases.

the aliphatic chain of the fatty acids. When n decreases, one approaches a critical point, as when the temperature is increased for a given acid; as a consequence, a simultaneous decrease of the size of the coexistence region occurs. The strong influence of the small ethyl head group on the behavior of C_{16}Et monolayers is also remarkable. The increase of the head size causes a strong expansion of the ester monolayer, leading to the appearance of a LE phase, while this phase does not exist for C_{16} [Fig. 2(b)].

B. Surface viscoelasticity

The dilational elasticity modulus ε and loss modulus $\omega\kappa$ of the monolayers of the four compounds, as obtained from electrocapillary experiments, are presented in Figs. 3–6. In the following, we will discuss the rheological characteristics of the different phases of the monolayer.

G-LE coexistence region

The *G*-LE region is characterized by very low values of the surface pressure, $\Pi\sim0$ within experimental uncertainty (±0.5 mN/m). For an area per molecule $A>60\,\text{Å}^2$, the capillary waves propagate as on the clean surface of the pure aqueous subphase. For a smaller molecular area, we have observed a modulation of the sinusoidal envelope of the spatial surface profile (see Fig. 7). This could reflect the inhomogeneous character of the monolayers, with regions of different wave damping [38]. However, the modulation scale is of the order of a centimeter, while the characteristic size of LE domains is of the order of a few tenths of a micron, as evidenced from BAM and FM characterization [29]. The modulation of the surface profile could be due to the convective motion of the gaseous domains and to their size polydispersity. Similar modulation phenomena have been already observed at similar frequencies in C_{14} and C_{15} monolayers by Noskov and Zubkova [39], and at higher frequencies with light scattering experiments, for the monolayers of the same acids by Hard and Neumann [40] and in C_{15} monolayers by Winch and Earnshaw [41]. In this latter work a series of experiments was undertaken in order to estimate the effect of the domains mobility: this leads to an apparent diameter of the inhomogeneities of the order of 1 cm as in our experiments. In the case of the C_{16}Et monolayer, modulations of the surface profile have not been observed, may be because the propagation characteristics of the capillary waves in the LE phase are closer to the values for the pure subphase than in the case of fatty acids. No data are available for palmitic acid C_{16}, that do not show a LE phase at the room temperature.

LE phase

When entering the LE region, a sudden increase of ε is observed for the fatty acid monolayers. The transition is much more gradual for the more expanded ester monolayers. The dilational elasticity ε of the LE phase is between 15 and 20 mN/m for C_{15} [see Fig. 4(a)]; 13 and 35 mN/m for C_{14} [see Fig. 3(a)]; and 0 and 20 mN/m for C_{16}Et [see Fig. 6(a)]. There are no experimental results for C_{16} since the LE phase is not found at room temperature. These results are very similar to those obtained from QESLS for C_{14} [40,42,43] and C_{15}, [40–42]. Hence, in the range 10^2-10^6 Hz, the dilational elasticity seems to be frequency independent.

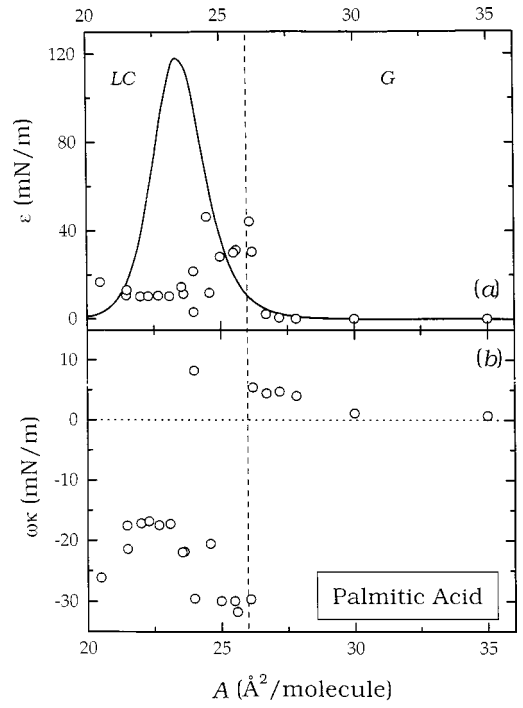

FIG. 5. Experimental viscoelasticity data for the monolayers of palmitic acid C_{16} at the air-water interface and at 22 ± 1 °C as a function of area per monomer. (a) Dilational elasticity modulus $\varepsilon(\omega)$ at $\nu=800$ Hz and comparison with the static value ε_0 (continuous line). (b) Dilational loss modulus $\omega\,\kappa(\omega)$ at the same frequency. The vertical dotted lines delimit the different 2D phases.

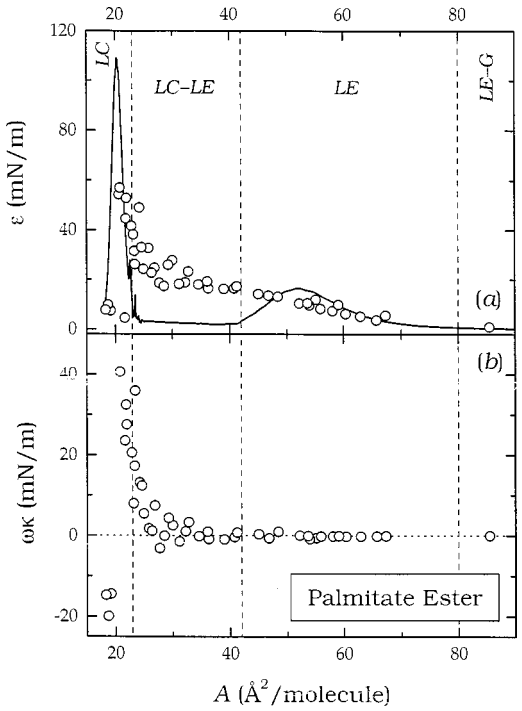

FIG. 6. Experimental viscoelasticity data for the monolayers of palmitic ethyl ester C_{16}Et at the air-water interface and at 22 ±1 °C as a function of area per monomer. (a) Dilational elasticity modulus $\varepsilon(\omega)$ at $\nu=800$ Hz and comparison with the static value ε_0 (continuous line). (b) Dilational loss modulus $\omega\,\kappa(\omega)$ at the same frequency. The vertical dotted lines delimit the different 2D phases.

The situation is less clear for the surface viscosity, especially in the lower frequency domain. For C_{15} [see Fig. 4(b)], the dilational viscosity is small, but negative: $\omega\kappa$ decreases to about -10 mN/m at $A=35$ Å^2, where LC domains begin to nucleate. The decrease of viscosity upon compression is even more pronounced in the case of C_{14} [see Fig. 3(b)], $\omega\kappa$ reaching -18 mN/m for the highest LE concentration. On the other hand, the surface viscosity of the ester monolayers stays equal to zero in the whole LE phase region [see Fig. 6(b)].

Noskov and Zubkova [39] studied C_{14} and C_{15} monolayers in the same frequency domain by using a mechanical excitation instead of the electrocapillary method. They also obtained negative values of the dilational viscosity in this domain, although in a rather complicated way. Since their damping and wavelength data were too scattered to allow the direct calculation of ε and $\omega\kappa$, they looked for values of the viscosity which give back the measured values of damping, and used the static elasticity as calculated from the slope of the Π-Γ isotherms [see Eq. (5)] [39],

However, in all high frequency studies by the QESLS method [40–42,44], small positive values for the loss modulus $\omega\kappa\sim1$ mN/m are reported. It thus seems that the viscous contribution to the dilational modulus in the LE phase is negligible in that frequency region. Let us quote an exception: Sakai and Takagi [43] obtained $\omega\kappa\sim10$ mN/m for C_{14} monolayers in the LE phase.

LE-LC coexistence region

In this two-phase region, ε increases progressively from a pure LE value at a low density boundary to a pure LC value at a high density boundary for C_{15} and C_{16}Et monolayers. As pointed out by Miyano [45], the measurement of the averaged properties is only possible when the scale of heterogeneity is less than the wavelength. Here the domains dimensions observed by FM in the C_{14} [46] and C_{15} [47] monolayers are of the order of ~100 μm, small compared to the wavelength of capillary waves (about 0.2 mm for $\omega=800$ Hz). However, since the spatial distribution of the domains is probably heterogeneous, the experimental data in this two-phase region are scattered. In the case of C_{14}, the dilational elasticity fluctuates even more than for other compounds with a tendency to decrease. This particular behavior will be discussed later.

The elasticity deduced from QESLS measurements for C_{14} [40,42] and C_{15} [41] is also intermediate between the values obtained for the two coexisting phases. The error bar is large as well, but the wavelength is much shorter in these experiments ($\lambda=10-500$ μm), thus comparable with domain dimensions.

The problem of the dilational modulus of a composite surface was theoretically addressed by Lucassen [48]. If line tensions are neglected, the apparent modulus of a composite surface with condensed and expanded domains occupying A_C and A_E partial areas, respectively, is given by [48]

$$\frac{1}{\varepsilon}=\frac{1}{d\gamma}\frac{dA_{\mathrm{Tot}}}{A_{\mathrm{Tot}}}=\frac{1}{d\gamma}\left(\frac{dA_E}{A_{\mathrm{Tot}}}+\frac{dA_C}{A_{\mathrm{Tot}}}\right)=\frac{\phi}{\varepsilon_E}+\frac{1-\phi}{\varepsilon_C}, \quad (6)$$

where $A_{\mathrm{Tot}}=A_E+A_C$. In this expression ϕ represents the fractional area occupied by the expanded phase, which here

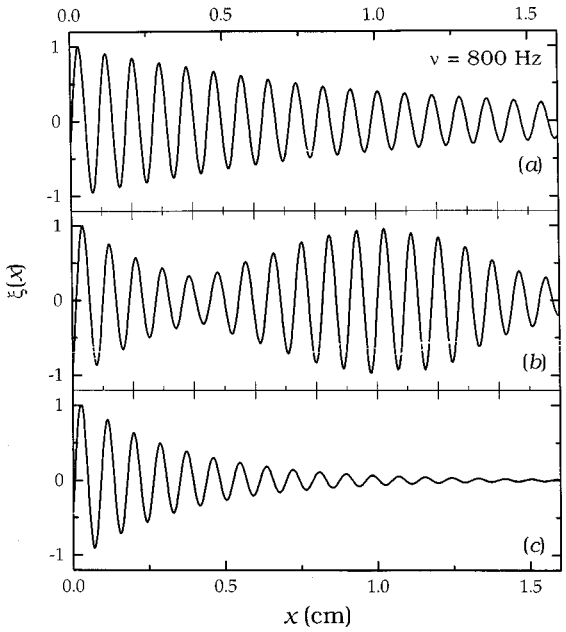

FIG. 7. Experimental spatial profile of an externally excited electrocapillary wave at $\nu = 800$ Hz for a pentadecanoic acid monolayer spread at the air-water interface: (a) in the diluted region at $A = 65$ Å^2/monomer, (b) in the G/LE coexistence region at $A = 47$ Å^2/monomer, and (c) in the LE monophasic region at $A = 40$ Å^2/monomer.

is the continous phase $\phi = A_E/(A_E + A_C)$; ε_E and ε_C are the elasticities of the homogeneous expanded and condensed phases, respectively. Equation (6) obviously applies only if the time scale of the area variation is short compared to the time required for the transformation of the LE domains into LC domains, or inversely. Evaluations of ϕ from FM image analysis were made by Suresh, Nittman and Rondelez [46] for C_{14} and Moore *et al.* [47] for C_{15} monolayers. In this last work [47], it was shown that ϕ can be described by a lever rule, and that the molecular area in the coexisting phases could be obtained from extrapolation to $\phi = 0$ and $\phi = 1$ [47]:

$$\phi = \frac{A_E}{A_C + A_E}, \quad A_E = \frac{\phi}{1-\phi} A_C \tag{7}$$

We have calculated the fractional area of the expanded continuous phase ϕ from the dynamic elasticity data by applying Eq. (6). The results for C_{15} and C_{16}Et monolayers are represented in Fig. 8 as a function of the total surface concentration $\Gamma = 1/A_{\mathrm{Tot}}$. The calculated liquid expanded fraction ϕ follows closely the expected linear dependence: $\phi = A_E\Gamma$. The intersections with the horizontal axes at $\phi = 1$ and 0 are also in excellent agreement with the limits of the LE-LC coexistence region, represented by the arrows in this figure, as obtained from the isotherms and the FM experiments (see Table I). This results confirm the linear Γ dependence of the fractional area ϕ, previously found by Moore *et al.* [47], as well as the validity of the Lucassen model for the composite elasticity [48].

As far as viscosity is concerned, our data show that compression of the fatty acid monolayers leads to more negative $\omega\kappa$ values [see Figs. 3, 4, and 5(b)]. The viscosity of the

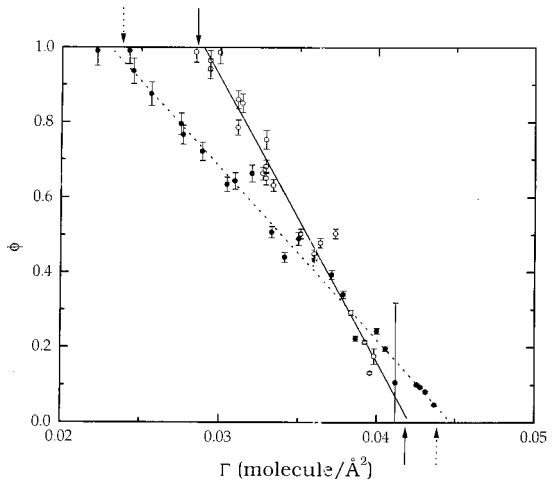

FIG. 8. Fractional area occupied by the expanded phase (continuous phase) ϕ, calculated from Eq. (6), as a function of the monolayer density $\Gamma = 1/(A_E + A_C)$ in the LE/LC coexistence region. (○) Myristic acid and (●) pentadecanoic acid. The lines represent the fit of these data to the linear dependence $\phi = A_E\Gamma$. The boundaries of the coexistence region obtained independently from the equilibrium Π-A data are represented by the arrows.

ester remains close to zero also in this regime [see Fig. 6(b)]. In the higher frequency region (QESLS data), positive values of the dilational viscosity for fatty acids were reported, together with their increase upon compression.

Condensed LC and SL phases

In the condensed phases, there is a striking difference between the viscoelastic behavior of fatty acids and ester monolayers. In the ester case, ε increases suddenly from about 20 mN/m at 23 Å^2 to about 60 mN/m for the collapsed monolayer, as shown in Fig. 6(a). In the same way, $\omega\kappa$ increases from zero to 60 mN/m. Such a strong increase has been already observed for the monolayers of heneicosanoic acid (C_{21}) for the two components of the complex shear modulus, measured with the torsion pendulum [49]. It is then quite probable that the main contribution to the viscoelasticity of the ester originates from the shear modulus. However, in the case of shear viscoelasticity of heneicosanoic acid there are discontinuities at the $L2/L2'$ and $L2'/S$ phase transitions, whereas in the case of ester, shear plus dilational elasticity and viscosity increase monotoneously [49]. When collapse is reached, both coefficients decrease: the elasticity to a very small value (below 10 mN/m), and the viscosity becomes negative. This drop in viscoelasticity at monolayer collapse is also found with fatty acids, for which, however, the decrease of elasticity and viscosity starts long before collapse.

The viscoelastic behavior of the C_{16} monolayer is noticeably different (see Fig. 5). In the high density side of the G-LC coexistence region, $\omega\kappa$ starts to increase, whereas ε remains practically zero. After compression to the LC phase at 26 Å^2, ε grows suddenly while a quasidiscontinuous jump to negative values is observed for $\omega\kappa$. However, two distinct regions are clearly distinguished in this concentration regime: between 26 and 23 Å^2, the elasticity is high ($\varepsilon \sim 30$ mN/m) and the viscosity strongly negative ($\omega\kappa \sim -30$ mN/m), and below 23 Å^2 the elasticity drops to 10

mN/m and $\omega\kappa$ increases to about -20 mN/m.

A plausible explanation for this behavior lies in the in-plane shear contribution to the dilational modulus. For the uniaxial compression applied in the experiments, the elasticity modulus contains both pure dilational and shear contributions, the latter becoming important only for highly condensed or solid phases. It has been found that the shear viscosity, measured by a torsion method at low frequency ($\sim$1 Hz), increases by two orders of magnitude when fatty acids monolayers enter the LC phase [34]. This is in apparent contradiction with the strong negative values of $\omega\kappa$. However, more recently Gaub and McConnell [50] reported apparent negative values for the shear viscosity of C_{15} monolayers at $\sim$10 Hz, in the region where we observe the smallest κ values (26–23 Å^2). Below 23 Å^2, the shear viscosity becomes positive and grows very quickly. Consequently, the dilational viscosity variation could be qualitatively accounted for by the shear viscosity contribution. In their study of C_{21}, Ghaskadvi *et al.* [49] reported a nonlinear behavior in this region, which could possibly also affect dilational parameters. The comparison with the QESLS data is not conclusive, since these measurements were not performed close enough to the saturation and collapse of the monolayer. Hard and Neumann [40] did not study a molecular area smaller than the ones corresponding to the maximum elasticity in our measurements, below which the dilational viscosity changes sign. The high frequency dilational elasticity increases upon compression and reaches 80 mN/m for C_{14} and 120 mN/m for C_{15}, values systematically higher than the maximum elasticity obtained in our measurements (40 and 100 mN/m, respectively). This indicates the existence of a faster relaxation process. Likewise, the viscosity obtained from QESLS increases upon compression, with maximum $\omega\kappa$ values of 2 and 20 mN/m for C_{14} and C_{15}, respectively. The Hard-Neumann results [40] were confirmed later by Winch and Earnshaw for C_{15} [41]. Byrne and Earnshaw found some evidence of a drop in elasticity in the highest density region of C_{15} and C_{14} monolayers [42].

IV. DISCUSSION

Let us first compare the dynamic elasticity of the studied Langmuir films with the static one ε_0:

$$\varepsilon_0 = \lim_{\omega \to 0} \left(\frac{\partial \gamma}{\partial \ln A} \right) = - \left(\frac{\partial \gamma}{\partial \ln \Gamma} \right). \tag{8}$$

If there are no in-plane relaxation processes at frequencies smaller than the one studied and no exchanges with the bulk, $\varepsilon(\omega) = \varepsilon_0$. This static elasticity modulus has been calculated after numerical derivation of the smoothed Π-A equilibrium curves in Fig. 2(a) and 2(b). Similar values are deduced from the curves of Fig. 2(c) obtained from continuous compression. Positive differences between the dynamic elasticity ε and the static one ε_0 suggest the occurrence of relaxation processes within the monolayer plane, or of shear contributions, nonzero only for dense phases. If a relaxation occurs it will be accompanied by nonzero values of the loss modulus.

As it can be seen in Figs. 7 and 3, the dynamic elasticity very slightly exceeds the static limit in the LE state of the fatty acid monolayers. Unfortunately, since the dilational viscosity exhibits zero or small negative values in this regime it is not possible to evaluate the relaxation time with classical expressions such as Maxwell viscoelastic equations [51].

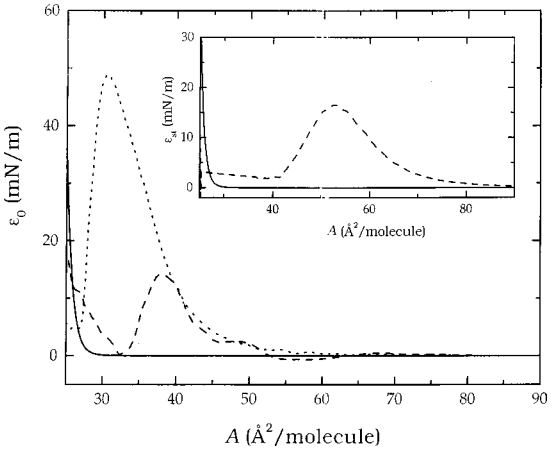

FIG. 9. Comparison of the static limit of the dilational elasticity modulus or thermodynamic isothermal compressibility $\varepsilon_0 = A(\partial\gamma/\partial A)_T$ for the three studied fatty acids: (——) palmitic C_{16}, (— — —) pentadecanoic C_{15}, and (· · · ·) myristic C_{14}. The inset shows the differences between the static compressibility of the monolayers of (——) palmitic acid and (— — —) its ethyl ester C_{16}Et.

Figure 9 shows the values of ε_0 for the fatty acid monolayers in the high dilution region (*G*-LE). One sees that when *n* decreases, the maximum of the static elasticity increases and shifts to smaller molecular areas. The maximum occurs at the molecular density at which excluded area effects become important, announcing the transition to the LC state. From a microscopic point of view, the observed behavior correlates well with a probable increase of molecular tilt as *n* decreases. The extreme case corresponds to palmitic acid, whose chains adopt a nearly vertical all-trans conformation and does not have an expanded liquid phase. The introduction of the small ethyl group in C_{16}Et probably restores a tilt and thus the LE phase.

Upon further compression, the monolayer undergoes the LE-LC transition, where the surface pressure remains constant, implying a static modulus equal to zero. The dynamic values however are non zero, both in our experiments and in QESLS ones [40,42]. Obviously, a relaxation process occurs here also, but since $\varepsilon - \varepsilon_0$ is independent on frequency, slow collective motions should be responsible for the observed difference ($\omega\tau \gg 1$). In such a composite surface, a possible relaxation mechanism is the change of the domain size or shape upon compression. In their study of C_{14} monolayers, Suresh, Nittmann, and Randelez [46] observed diffusion controlled growth of the domains, i.e., transport of matter between the condensed domains and the expanded ones through surface diffusion. The characteristic time of this mechanism is $\tau = 1/(D_S\ q^2)$, D_S being the surface diffusion coefficient, of the order of 10^{-7} and 10^{-9} cm^2/s in LE and LC phases, respectively [52]. Here $q \sim 100\,\mathrm{cm}^{-1}$, leading to $\tau \sim 10^3 - 10^5$ s. Domain shape changes, on the other hand, would be controlled by the line tension λ [53]. The line tension λ should be smaller for the near-critical monolayers of C_{14} (only 9 °C below the critical temperature), so the relaxation of any strain due to a shape deformation should be

easier. We come here to one of the key points of our argumentation: if a compression-induced shape transition (monophasic fluid stripe phase) was responsible for the existence of negative dilational viscosities, it would occur more easily close to a critical point.

In the condensed states of fatty acids monolayers, ε increases and reaches, maximum close to collapse area $\sim$19–20 Å^2. The QESLS dynamic elasticities are larger than those for the smaller frequencies studied here, and larger than the static ones. This indicates the presence of new relaxation effects, faster than in the LE region.

In the collapse region, we invariably observe a drop of elasticity and appearance of negative viscosities, even for the monolayer of palmityl ethyl ester. This behavior is very different from that seen (and theoretically predicted) by Veer and van den Tempel [54] for monolayers of fatty alcohols. Such a behavior has been modeled by assuming a first order rate process for the diffusive exchange of surfactant between the tridimensional crystals and the monolayer. The collapse is predicted to be accompanied by an increase of the dilational elasticity and viscosity coefficients, $\omega\kappa$ sometimes being larger than ε.

The key to understanding negative viscosities seems hidden in the differences between ester and fatty acids monolayers. We will discuss further these differences as seen in BAM, FM, and x-ray studies. Möhwald [52] and McConnell [53] observed that monolayers of fatty acids, as well as those of some lipids, are able to develop complex domain structures in the LE-LC coexistence region. These structures result from a competition between long range electrostatic (dipolar) forces and line tension [53]. The electrostatic energy depends on the domain shape and density, and decreases with the domain size. However, the line tension contribution increases if the number of domains increases. McConnell [53] and Seul and Andelman [21] showed that the interplay between these two energetic contributions is responsible for shape transitions. Upon compression, the circular shape typical of domains in the LE-LC coexistence region becomes unstable; the domains first adopt ellipsoidal shapes, and finally transform into thin long stripes. At higher molecular density, the electrical repulsion between domains prevents them from fusing and allows the formation of lamellar or hexagonal bidimensional superlattices [21,53]. These macroscopically modulated phases were predicted theoretically for Langmuir monolayers at thermodynamic equilibrium in Refs. [26, 29]. Visual observation of these textures at room temperature is possible only in metastable states obtained after mechanical compression of the monolayer. However, the stripe textures develop spontaneously in monolayers of C_{14} and C_{15} at low enough temperatures, normally below the triple point ($T_t \sim 5$ °C for C_{14} and $\sim$17 °C for C_{15}). In the case of C_{14}, aligned stripes have sometimes been observed even at 12 °C [23]. The stripes tend to be aligned perpendicular to LE-LC boundaries, and grow primarily by diffusion [23]. From the polarization analysis of the refraction index variations of the BAM images, Ruiz-Garcia *et al.* [23] concluded that these stripe structures are associated to a spatial modulation of the molecular tilt azimuth.

In the ester case, the domains have a well defined substructure, with a sixfold division. In each of the six segments, the molecules have a uniform orientation, different from that of the other segments. It can be concluded that it is easier to cross the LE-LC boundary upon compression/expansion in the case of fatty acids, where the orientation of the molecules changes continuously inside the domains.

TABLE III. Molecular tilt in the condensed LC (liquid condensed) and SL (superliquid) phases of the studied surfactants at the air-water interface (data from Ref. [32]).

Surfactant	T (°C)	Π (mN/m)	Phase	Tilt azimuth (deg)
C_{14}	10	$\sim$5	LC (NN)[a]	27
	10	$\sim$20	LC (NN)	9
	10	$\sim$22	SL	0
C_{16}	24	$\sim$10	LC (NN)	25
	24	$\sim$18	LC (NNN)[b]	16
	24	$\sim$22	SL	0
C_{16}Et	20	$\sim$6	LC (NNN)	9
	20	$\sim$8	SL	0

[a]NN—chains tilted toward nearest neighbors.
[b]NNN—chains tilted toward next-nearest neighbors.

In equilibrium conditions, and at room temperature, the domains in fatty acid monolayers are rather circular in shape. However, in our experimental conditions, with a relative area modulation $u_x \sim \Delta A/A \sim 5\,10^{-5}$, we have a compression-expansion rate of about 3 Å^2/molecule sec, which is at least one order of magnitude greater than the highest rates used in mechanical compression experiments, where kinetic effects are important. In addition, it is well known that during the nucleation period, an increase of the compression rate, which causes a larger deviation from the equilibrium pressure, also increases the number of nuclei. Therefore, the capillary waves might be able to create a stripe structure. If such an induced phase transition occurs, energy transfer from the capillary to the longitudinal waves could occur: after phase separation, the resulting increase in chemical free energy can be transferred back to the capillary wave, leading to a decrease of its damping. The free energy cost to create a critical nucleus of the ordered phase should be reduced in the case of the C_{14} monolayer due to decrease of the line tension close to the critical point. It should then be easier to induce the formation of a stripe phase, even in a region outside of the metastability region (between the binodal and the spinodal), and, indeed, negative dilational viscosities are already found in the pure LE phase region close to the binodal. It is less evident to account for negative viscosities in the concentrated phases region; however, a similar explanation can be tentatively proposed.

In Table III, the sequence of appearance of the different condensed phases is presented for some compounds. These data have been recently obtained from grazing incidence X-ray diffraction and BAM experiments [32]. Two particularities concerning the C_{16}Et monolayers can be noticed. The first one concerns the LE-LC phase transition. For fatty acids, the LC phase is a nearest-neighbor tilted phase, whereas for the ester a more ordered next-nearest-neighbor tilted LC phase with a small polar tilt angle is obtained upon compression. In general, fatty acids differ from their esters by a higher polar tilt angle with a higher dispersion of the tilt azimuth at the air-water interface. The second particularity concerns the LC-SL phase transition, which occurs at rela-

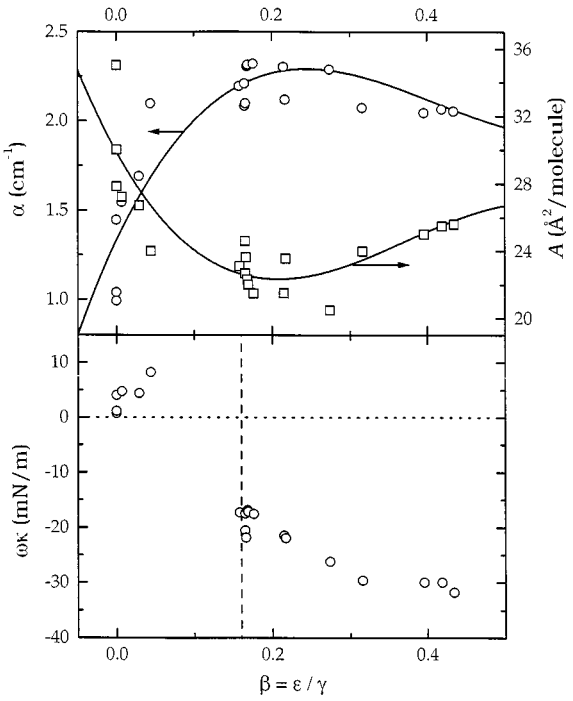

FIG. 10. (a) Spatial damping coefficient α for the palmitic acid monolayer at $T=20\,^{\circ}\mathrm{C}$ as a function of the experimental values of the elasticity ratio $\beta=\varepsilon/\gamma$. For the sake of comparison with the data in Fig. 5, the values of molecular area are also shown in the right vertical scale. The continuous lines are only a visual guide. (b) Dilational loss modulus $\omega\kappa$ at $\nu=800\,\mathrm{Hz}$ as a function of β. Note that negative values are only found at $\beta\geqslant\beta_{\mathrm{res}}\sim 0.16$ (vertical dashed line). This condition implies $A\leqslant 26\,\mathrm{Å}^2$ (see Fig. 5).

tively low surface pressure ($\sim$6 mN/m) for the esters as compared to fatty acids ($\sim$22 mN/m). This leads us to conclude that the transition to stripe phases is easier for fatty acid monolayers than for the esters.

Let us finally consider the hydrodynamic aspects. As mentioned in Sec. I, the hydrodynamic coupling between transversal and longitudinal waves is more effective close to the resonance condition $\beta=\varepsilon/\gamma\sim 0.1-0.2$. This leads to a linear mode mixing at resonance, where energy transfer between modes is more effective [55]. As a result, the capillary damping coefficient is at a maximum at resonance. Figure 10 shows the damping coefficient of the capillary modes and the calculated values of dilational viscosity for the monolayer of palmitic acid. When the resonance condition is approached ($\beta\sim 0.16$), the capillary damping increases to its maximum value, in coincidence with a jump of $\omega\kappa$ to negative values. After this point, the condition for mode coupling is less optimal ($\beta\sim 0.4$); energy transfer is still possible, although less effective, possibly explaining why negative values of the dilational viscosity are still found. Similar results have been obtained for the other fatty acid monolayers.

When negative viscosities appear after the resonance condition, spatial profiles are distorted close to resonance [Fig. 7(b)]. The amplitude of the signal is modulated and does not decay exponentially. Rather than being due to surface inhomogeneities, as discussed in Sec. III B, this could be a clear signature of mode coupling.

We have attempted to observe directly the possible phase transition produced by the capillary wave. For this purpose, a Langmuir through with its electrocapillary excitation device was installed in a BAM setup. We were unable to observe any stripe phase. However, this only means that the lifetime of the stripes, if they are produced, is shorter than the time required to obtain a BAM image ($\sim$1 s). This is consistent with the fact that the energy transfer should follow the wave excitation, i.e., be fast.

V. CONCLUSIONS

Negative values of the dilational viscosity, experimentally observed in soluble and insoluble monolayers, might be caused by phase transitions induced by the propagation of the surface waves. A clear correlation between this *exotic* viscoelastic behavior and the phase diagram has been evidenced. The proximity of the 2D LE-LC critical point, where strong monolayer density fluctuations occur, is one key point in the appearance of negative κ values. The particular morphology and structure of the phases also seem to play decisive roles. In particular, the role played by the molecular tilt is a second key point. Finally, there is a third point, the coupling between longitudinal and capillary modes, which seems to facilitate the decrease of the viscous dissipation, especially near resonance conditions. When the three conditions are simultaneously present, very negative effective dilational viscosities can be obtained, as in the case of myristic acid monolayers.

Experiments on other systems are needed to confirm these ideas. In particular, the extension of the frequency range will be helpful to clarify the relaxation aspects.

ACKNOWLEDGMENTS

F.M. thanks European Commission for financial support under Contract No. FMBICT960872. Dr. C. Mingotaud (CRPP, France) is gratefully acknowledged for his help with the BAM instrument. We thank also Professor R. G. Rubio (UCM, Spain) for fruitful discussions on phase coexistence and metastable states.

[1] M. van den Tempel and E. H. Lucassen-Reynders, Adv. Colloid Interface Sci. **18**, 281 (1983); E. H. Lucassen-Reynders, in *Anionic Surfactants, Physical Chemistry of Surfactant Action*, edited by E. H. Lucassen-Reynders (Dekker, New York, 1981).

[2] V. G. Levich, *Physicochemical Hydrodynamics* (Prentice-Hall, Englewood Cliffs, NJ, 1962).

[3] E. H. Lucassen-Reynders and J. Lucassen, Adv. Colloid Interface Sci. **2**, 347 (1969).

[4] M. Van den Tempel, J. Non-Newtonian Fluid Mech. **2**, 205 (1977).

[5] C. H. Sohl, K. Miyano, and J. B. Ketterson, Rev. Sci. Instrum. **49**, 1464 (1978).

[6] C. Stenvot and D. Langevin, Langmuir **4**, 1179 (1988).

[7] J. Mann, Jr. and R. S. Hansen, J. Colloid Interface Sci. **18**, 757 (1963).
[8] B. A. Noskov and D. O. Grigoriev, Prog. Colloid Polym. Sci. **97**, 1 (1994).
[9] *Light Scattering by Liquid Surfaces and Complementary Techniques*, edited by D. Langevin, Surfactant Sci. Series, Vol. 41, (Dekker, New York, 1992).
[10] L. Kramer, J. Chem. Phys. **55**, 2097 (1971).
[11] J. Lucassen and M. Van den Tempel, Chem. Eng. Sci. **27**, 1283 (1972).
[12] H. C. Maru and D. T. Wasan, Chem. Eng. Sci. **34**, 1295 (1979).
[13] J. C. Earnshaw and E. McCoo, Langmuir **11**, 1087 (1995).
[14] S. K. Peace, R. W. Richards, and N. Williams, Langmuir **14**, 667 (1998).
[15] D. Sharpe and J. Eastoe, Langmuir **12**, 2303 (1996).
[16] X. Chu and M. Velarde, Phys. Chem. Hydrodynamics **10**, 727 (1988); J. Colloid Interface Sci. **131**, 471 (1989).
[17] M. Hennenberg, X. L. Chu, A. Sanfeld, and M. G. Velarde, J. Colloid Interface Sci. **150**, 7 (1992).
[18] D. M. A. Buzza, J. L. Jones, T. C. B. McLeish, and R. W. Richards, J. Chem. Phys. **109**, 5008 (1998).
[19] F. Monroy, J. Giermanska-Kahn, and D. Langevin, Colloids Surf., A **143**, 251 (1998).
[20] F. Monroy, J. Giermanska-Kahn, and D. Langevin (unpublished).
[21] M. Seul and D. Andelman, Science **267**, 476 (1995).
[22] S. B. Dierker, R. Pindak, and R. B. Meyer, Phys. Rev. Lett. **56**, 1819 (1986).
[23] J. Ruiz-Garcia, X. Qiu, M. W. Tsao, G. Marshall, C. M. Knobler, G. A. Overbeck, and D. Möbius, J. Phys. Chem. **97**, 6955 (1993).
[24] S. Rivière, S. Hénon, and J. Meunier, Phys. Rev. E **49**, 1375 (1994).
[25] M. Seul and S. V. Chen, Phys. Rev. Lett. **70**, 1658 (1993).
[26] D. Andelman, F. Brochard, and J. F. Joanny, J. Chem. Phys. **86**, 3673 (1987).
[27] J. V. Selinger, Z. G. Wang, R. F. Bruinsma, and C. M. Knobler, Phys. Rev. Lett. **70**, 1139 (1993).
[28] J. G. Hu and R. Granek, J. Phys. (France) **6**, 999 (1996).
[29] C. M. Knobler, Adv. Chem. Phys. **77**, 397 (1990).
[30] A. M. Bibo, C. M. Knobler, and I. R. Peterson, J. Phys. Chem. **95**, 5591 (1991).
[31] A. M. Bibo and I. R. Peterson, Adv. Mater. **2**, 309 (1990).
[32] G. Weidemann, G. Brezesinski, D. Vollhardt, F. Bringern, K. de Meijere, and H. Möhwald, J. Phys. Chem. B **102**, 148 (1998).
[33] W. D. Harkins and E. Boyd, J. Phys. Chem. **45**, 20 (1941).
[34] E. Boyd and W. D. Harkins, J. Am. Chem. Soc. **61**, 1189 (1939).
[35] O. Albrecht, H. Matsuda, K. Eguchi, and T. Nakagiri, Thin Solid Films **338**, 252 (1999).
[36] A. Fisher and E. Sackmann, J. Colloid Interface Sci. **112**, 1 (1985).
[37] G. L. Gaines, *Insoluble Monolayers at Liquid-Gas Interfaces*, (Wiley, New York, 1966).
[38] Q. Wang, A. Feder, and E. Mazur, J. Phys. Chem. **98**, 12 720 (1994).
[39] B. A. Noskov and T. U. Zubkova, J. Colloid Interface Sci. **170**, 1 (1995).
[40] S. Hard and R. D. Neumann, J. Colloid Interface Sci. **83**, 315 (1981); **120,**15, (1986).
[41] P. J. Winch and J. C. Earnshaw, J. Phys.: Condens. Matter **1**, 7187 (1989); J. C. Earnshaw and P. J. Winch, *ibid.* **2**, 8499 (1990).
[42] D. Byrne and J. C. Earnshaw, J. Phys. D **12**, 1145 (1979).
[43] K. Sakai and K. Takagi, Jpn. J. Appl. Phys., Part 2 **31**, L1488 (1992).
[44] Y. L. Chen, M. Sano, M. Kawaguchi, H. Yu, and G. Zografi, Langmuir **2**, 349 (1986).
[45] K. Miyano, Langmuir **6**, 1254 (1990).
[46] K. A. Suresh, J. Nittmann, and F. Rondelez, Europhys. Lett. **6**, 437 (1988).
[47] B. G. Moore, C. M. Knobler, S. Akamatsu, and F. Rondelez, J. Phys. Chem. **94**, 4588 (1990).
[48] J. Lucassen, Colloids Surf., A **65**, 139 (1992).
[49] R. S. Ghaskadvi, J. B. Ketterson, and P. Dutta, Langmuir **13**, 5137 (1997); R. S. Ghaskadvi, T. M. Bohanon, P. Dutta, and J. B. Ketterson, Phys. Rev. E **54**, 1770 (1996).
[50] H. E. Gaub and H. M. Mc Connell, J. Phys. Chem. **90**, 6830 (1986).
[51] L. D. Landau and E. M. Lifshitz, *Theory of Elasticity* (Pergamon, Oxford, 1986).
[52] H. Möhwald, Annu. Rev. Phys. Chem. **41**, 441 (1990).
[53] H. M. Mc Connell, Annu. Rev. Phys. Chem. **42**, 171 (1991).
[54] F. A. Veer and J. van den Tempel, J. Colloid Interface Sci. **42**, 418 (1972).
[55] J. C. Earnshaw and A. C. McLaughlin, Proc. R. Soc. London, Ser. A **433**, 663 (1991); **440**, 519 (1993).